Performance of NIR InGaAs imager arrays for science applications

S. Seshadri[a], D.M. Cole[a], B. Hancock[a], P. Ringold[a], C. Peay[a], C.Wrigley[a], M. Bonati[b], M.G. Brown[c], M. Schubnell[c], G. Rahmer[b], D. Guzman[b], D. Figer[d], G. Tarle[c], R.M. Smith[b], and C. Bebek[e]
[a]Jet Propulsion Laboratory, [b]California Institute of Technology, Pasadena, CA, [c]University of Michigan, Ann Arbor, MI, [d]Rochester Institute of Technology, Rochester, NY and [e]Lawrence Berkeley National Laboratory, Berkeley, CA, Department of Physics
MS 300-315, Jet Propulsion Laboratory, 4800 Oak Grove Drive, Pasadena, CA, USA 91109, Email: suresh.seshadri@jpl.nasa.gov; PH: (818)-354-8370

Despite its many potential advantages, the use of InGaAs-based arrays for scientific imaging in the near-infrared is minimal[1] and not widespread. For example, InGaAs imaging arrays are used in commercial Dense Wavelength Division Multiplexing (DWDM) telecommunications, military and aerospace applications.[2,3] In terms of performance, InGaAs detectors with high, flat QE already exist.[2] Technologically, a transparent InP substrate and substrate removal technology, such as that used to increase short wavelength performance and minimize cut-off wavelength non-uniformities and cosmic ray effects in HgCdTe, also exists. These advantages offer imagers based on InGaAs technology the potential to be a lower cost, higher reliability alternative to those based on HgCdTe. The work described herein provides more complete characterization of the low temperature performance of an InGaAs-based imager array than presently exists to assess the suitability of this technology for scientific imaging applications.

We characterized a nominally 1.7um cut-off wavelength 1kx1k InGaAs (lattice-matched to an InP substrate) photodiode array fabricated by Sensors Unlimited, Inc. (now Goodrich Corporation). The array was hybridized to a Rockwell H1RG multiplexer under the Lawrence Berkeley National Laboratory-led SuperNova/Acceleration Probe (SNAP) mission concept development program.[4,5,6] The detector was operated in the H1RG's slow readout mode, with buffered output, with an external current source.

The mean-variance and conversion gain (C_g) for the InGaAs detector are shown in Figures 1 and 2.[7] Note that the engineering definition of C_g (uV/e-) differs from the astronomers' definition (e-/DN, where DN=Digital Number or e-/ADU, where ADU=Analog-Digital Unit). We call the latter, the inverse gain (=1/C_g). From the figure, it is apparent that C_g is signal-dependent, with noticeable deviation from constancy at signal levels as low as 10-15 % of full scale. The interpixel capacitance factor was calculated to be 0.87, resulting in a ~13% gain error.[8,9] Thus, the resulting low signal *inverse* gain is 6.3 e-/DN. The measured linearity and full well, calculated using the conversion gain data, are illustrated in Figure 3. The full well for a 0.5V detector bias was calculated to be 435K e-.

Figure 4 illustrates the relative QE of the InGaAs detector at 140K. The curve has been adjusted to achieve the same maximum absolute 300K QE data. A nominal room temperature curve is also shown in the figure for comparison. It is evident that the spectral shape is retained, with the wavelength being shifted towards shorter wavelengths due to the band gap shift of the detector band edge. The shift corresponds to ~80nm shorter cut-off wavelength at 140K relative to 300K. This result is a bit higher than the ~100 nm shift expected using the 0.625 nm/K rate expected from theory.[10] However, the data correlates well with recent results obtained by others.[11]

Figure 5 illustrates histograms of the dark current at various temperatures. Figure 6 illustrates an Arrhenius plot of the temperature dependence of the mean dark current. The curve is relatively well behaved with an extrapolated value that matches nominal room temperature data. The calculated activation energy of 0.25 eV is a bit lower than the 0.37 eV expected for purely generation-recombination in the depletion region. The flattening of the dark current at low temperatures is thought to be due to the effect of photo-generation from diffuse cosmic rays in the InP substrate, as has been observed for non-substrate-removed HgCdTe.[6] Figure 7 illustrates the noise performance of the InGaAs focal plane array versus sampling depth. Secondly, while the electronics noise is well behaved, decreasing in line with the expected square root dependence with increasing Fowler sample, the excess detector noise does not. Persistence in the InGaAs detector, Figure 8, is seen to decay to <0.1% of the original signal level almost instantaneously, with a subsequent, well-behaved, 55 sec decay constant.

In conclusion, the low temperature performance of existing InGaAs detector technology is well behaved and sufficient for all but the most stringent scientific applications. The results presented are comparable to those obtained from existing HgCdTe imagers. The key differences observed are the magnitude of the temperature-

dependent shift in cut-off wavelength and the fact that the read noise is higher than that obtained for the most recently-developed HgCdTe.

ACKNOWLEDGEMENTS

The effort described herein was supported by funds from the JPL STI program. The detector development and procurement was sponsored by the United States Department of Energy under contract No. DE-AC02-05CH11231.

REFERENCES

1. R.J. van der A et al., *Low noise InGaAs infrared (1.0-2.um) focal plane arrays for SCIAMACHY*, SPIE Proceedings V2957, 1997, p54.
2. T. Martin, et al., *640-512 InGaAs focal plane array camera for visible and SWIR imaging*, Infrared Technology and Applications XXXI, edited by Bjørn F. Andresen,Gabor F. Fulop, Proc. of SPIE Vol. 5783 (SPIE, Bellingham, WA, 2005, p12.
3. A. Hoffman et al., *Megapixel InGaAs Arrays for Low Background Applications*, Infrared Technology and Applications XXXI, edited by Bjørn F. Andresen,Gabor F. Fulop, Proc. of SPIE Vol. 5783 (SPIE, Bellingham, WA, 2005, p32.
4. M.G. Brown, *Development of NIR Detectors and Science Driven Requirements for SNAP*, Astronomical Telescopes and Instrumentation 2006, Proc. SPIE 6265 paper 113.
5. M. Schubnell et al., *Near infrared detectors for SNAP*, Astronomical Telescopes and Instrumentation 2006, Proc. SPIE 6276 paper 29.
6. R. Smith, et al., *Noise and zero-point drifts in 1.7um cutoff detectors for SNAP*, Astronomical Telescopes and Instrumentation 2006, Proc. SPIE 6276 paper 30.
7. B. Pain and B. Hancock, *Accurate Measurement of Conversion Gain and Quantum Efficiency in CMOS Imagers*, IS&T/SPIE 15th. Annual Symposium, Sensors, Cameras, and Systems for Scientific/Industrial Applications Conference 5017A, January 22, 2003.
8. A. Moore et al., Proc. SPIE V. 5167 (2003).; A. Moore et al. *QE overestimation and Deterministic Crosstalk Resulting from Interpixel Capacitance*, Optical Engineering, V 45-7.; G. Finger, et al., *Conversion Gain and Interpixel Capacitance of CMOS Hybrid Focal Plane Arrays*, Proc. Scientific Detectors for Astronomy 2005, Eds. J.E. Beletic, P. Amico, Springer Astrophysics and Space Sciences Library, V336, 477-490.
9. Autocorrelation calculation performed by M. Bonati of California Institute of Technology, Department of Astronomy, Optical Observatories group.
10. V.A. Wilkinson and A.R. Adams, *The effect of temperature and pressure on InGaAs band structure*, Properties of lattice matched and strained InGaAs, P. Bhattacharya, ed., INSPEC EMI Series 8, 1993.
11. R. Guntupalli and R. Allen, *Evaluation of InGaAs camera for scientific near infrared imaging applications*, in Infrared and Photoelctronic Imagers and Detector Devices II, R.E. Longshore and A. Sood editors, Pric. SPIE V6294, (2006) p.1.

FIGURES

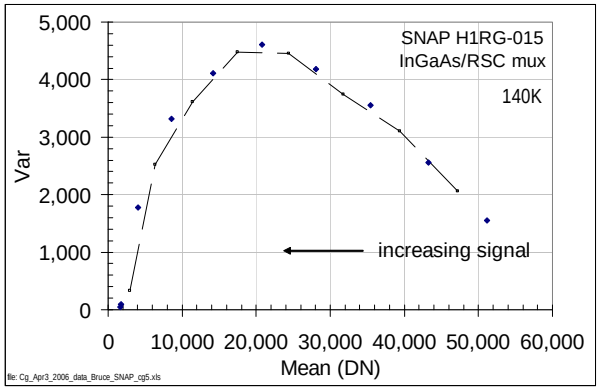

Figure 1: Mean-variance curve for an InGaAs detector biased at 0.5 V at 140K.

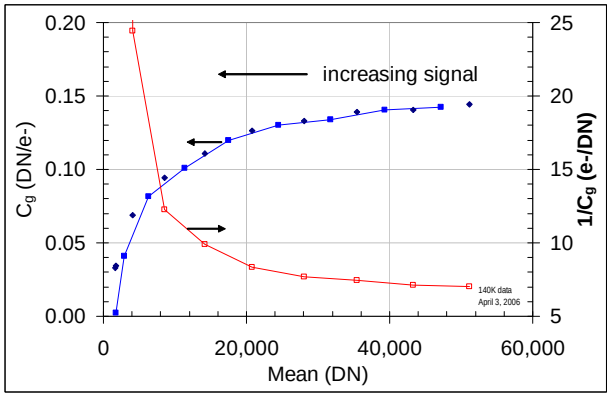

Figure 2: Conversion gain plot at 140K. Each data point represents a spatial average of 6-frame temporal variance from each of a 32x32 block of pixels.

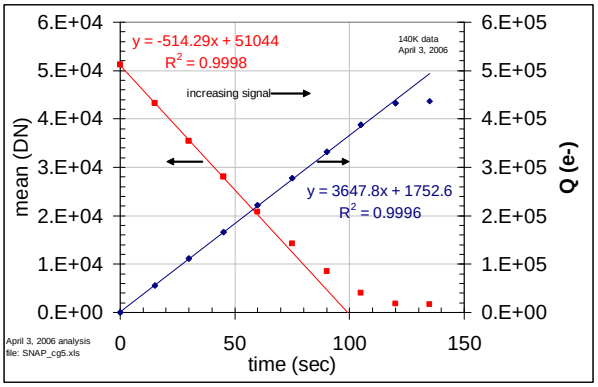

Figure 3: Linearity and full well of the InGaAs/mux hybrid package at 140K. The (red) line corresponds to a linear fit to the first 5 points in the mean data.

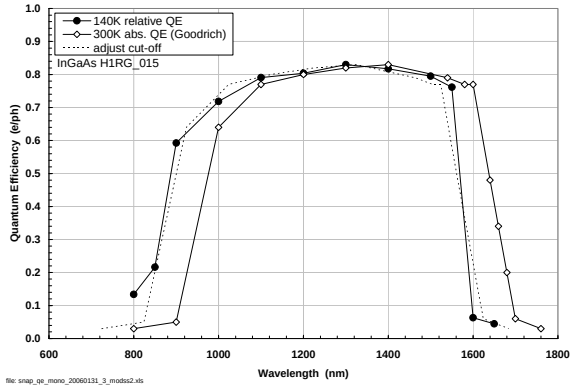

Figure 4: Relative quantum efficiency of the InGaAs detector at 140K. The dashed curve overlaying the 140K data is a copy of the 300K curve, shifted by 76 nm.

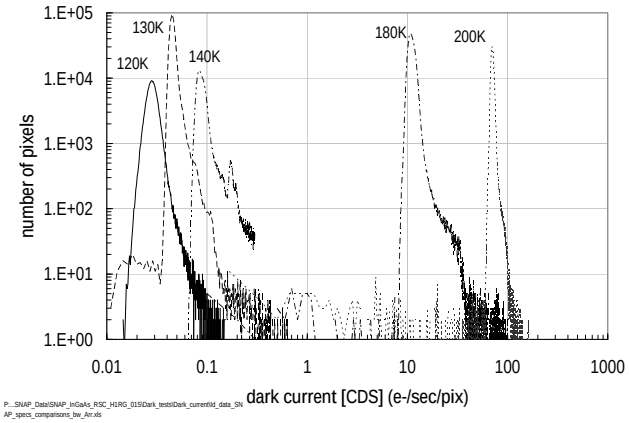

Figure 5: Dark current histograms at selected temperatures.

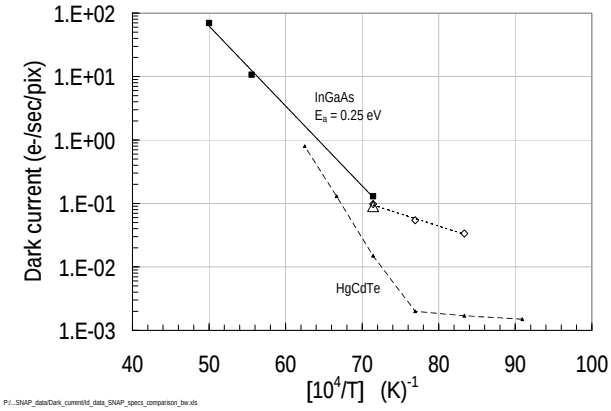

Figure 6: Arrhenius plot of dark current for InGaAs and state-of-the-art HgCdTe.

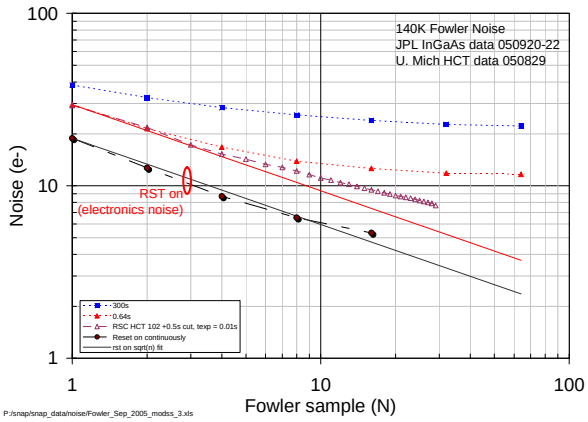

Figure 7: Noise vs number of samples at integration intervals of 0.64s and 300s. A curve of the electronics noise of our setup, scaled by C_g is shown for comparison.

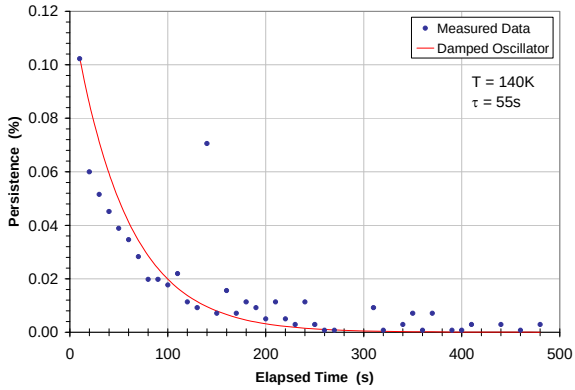

Figure 8: 140K persistence data for an InGaAs focal plane array. The initial illumination level was ~80% of full well.